Volume 3 | Number 3 | June 2016 | Pages 475–684

Environmental Science Nano

rsc.li/es-nano

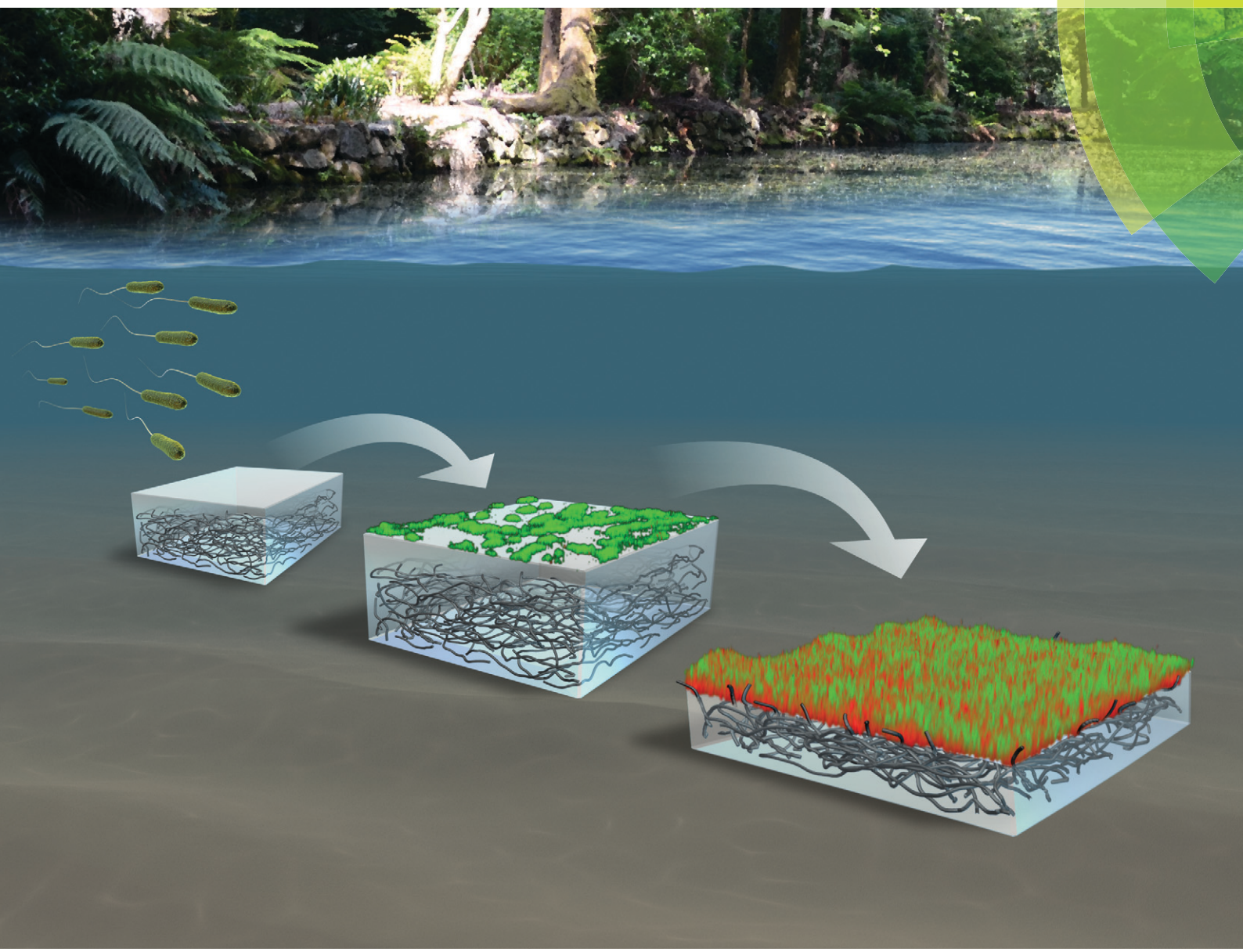

ISSN 2051-8153

ROYAL SOCIETY OF CHEMISTRY

PAPER
D. H. Fairbrother *et al.*
Biofilm development on carbon nanotube/polymer nanocomposites

175 YEARS

Environmental Science Nano

PAPER

View Article Online
View Journal | View Issue

Cite this: *Environ. Sci.: Nano*, 2016, **3**, 545

Biofilm development on carbon nanotube/polymer nanocomposites†

David G. Goodwin Jr.,[a] Z. Xia,[b] T. B. Gordon,[a] C. Gao,[c] E. J. Bouwer[b] and D. H. Fairbrother*[a]

Received 15th December 2015,
Accepted 27th April 2016

DOI: 10.1039/c5en00277j

rsc.li/es-nano

Biofilms have the potential to form on polymer nanocomposites containing carbon nanotubes (CNT/PNCs) when they come into contact with microorganisms in aqueous environments post-consumer use. In this study we explored the effect that CNT/PNC surface characteristics have on biofilm development, as compared to the unmodified polymer, under drip flow and static conditions. Specifically, we examined biofilm formation on CNT/PNCs where CNTs are initially present below the PNC surface but accumulate as a result of polymer biodegradation and where CNTs are initially present at the PNC surface. CNT/PNCs composed of oxidized multi-wall CNTs and poly-ε-caprolactone (PCL), a biodegradable polymer, were prepared and exposed to *Pseudomonas aeruginosa*; biofilm development was monitored using LIVE/DEAD staining. As prepared, CNTs were absent at the CNT/PCL surface, giving rise to an initially benign CNT/PCL-microbial interaction, analogous to that observed on PCL. As biofilm development progressed, however, PCL biodegradation caused CNTs to accumulate at the surface leading to an antimicrobial effect and eventually a full (2% w/w CNT) or partial dead (0.5% w/w CNT) layer of microorganisms. At later stages, active biofilm formation occurred on top of a protective layer of dead microorganisms indicating that biofilm growth on CNT/PCL nanocomposites was delayed, but not inhibited. CNTs also accumulated at CNT/PCL surfaces as a result of a simulated weathering process and these surfaces exhibited immediate cytotoxicity. However, "live-on-dead" biofilm formation was still ultimately observed. Qualitatively similar trends of biofilm development were observed under drip flow and static conditions although the structure and rates of biofilm formation differed.

Nano impact

Following consumer use, microorganisms will associate with and potentially form biofilms on carbon nanotube/polymer nanocomposite (CNT/PNC) surfaces in the environment. These CNT/PNC surfaces can have a range of different characteristics as a result of polymer matrix type, manufacturing method, wear during consumer use, or environmental transformations. This study shows that CNTs at the surface of a CNT/PNC are cytotoxic to microorganisms, and their presence causes a layer of dead cells to form, regardless of whether the CNTs are initially at the CNT/PNC surface or reach the surface as a result of polymer degradation during biofilm growth. CNT/PNCs used in consumer products therefore have the potential to be cytotoxic to microorganisms as the polymer matrix degrades. However, once CNTs at the surface are coated with a layer of dead cells, live-on-dead biofilm formation occurs under both static and low shear conditions, indicating that healthy biofilm growth on CNT/PCL nanocomposites will be delayed, but not prevented. The need for direct contact to be present between CNTs and microorganisms for cytotoxicity to occur will likely limit the use of CNT/PNCs in antimicrobial applications as biofouling will ultimately still occur. The existence of a dead layer of cells at the interface between the CNT/PNC and the active biofilm may, however, have implications for the physical stability of the biofilm (*e.g.* to sheer forces) and to the long term fate of the polymer itself (*e.g.* biodegradability).

[a] *Department of Chemistry, Johns Hopkins University, Baltimore, MD 21218, USA. E-mail: howardf@jhu.edu; Tel: +(410) 516 4328*
[b] *Department of Geography and Environmental Engineering, Johns Hopkins University, Baltimore, MD 21218, USA*
[c] *College of Chemistry, Jilin University, Changchun, 130012, China*

† Electronic supplementary information (ESI) available: XPS and TEM data, a schematic of OTS modification of glass slides and the spray-coating process, an illustration of the CNT/PNC photodegradation procedure, replicate SEM images, a picture of the drip flow reactor setup, replicate confocal laser scanning microscopy images of LIVE/DEAD stained *P. aeruginosa* on CNT/PCL nanocomposite samples and controls, biomass volume and biofilm thickness measurements made with COMSTAT 2, and an illustration of biofilm growth on 2% w/w O-MWCNT/PCL nanocomposites under static conditions. See DOI: 10.1039/c5en00277j

Introduction

Polymers, by virtue of their wide range of desirable properties and ease of production, are prevalent in every aspect of life ranging from familiar daily plastics such as rubber bands, garbage bags, and packaging materials to coatings used in the automobile and aerospace industries.[1–3] Incorporation of carbon nanotubes (CNTs) into polymers to prepare CNT/polymer nanocomposites (CNT/PNCs) has received increasing attention due to the beneficial material properties that CNTs can impart to polymers, greatly enhancing their range of potential applications. These improved properties can include high tensile strength, extraordinary hardness, and excellent thermal and electrical conductivity.[4–8] For this reason, industrial manufacturing of nanoproducts for consumer use, typically within the range of 1–5% w/w CNTs, is already underway for applications that include electronic devices, charge-dissipating packaging, fuel tanks, and anti-biofouling surfaces.[9–12]

Since plastic products that include CNT/PNCs will eventually enter the environment at the end of their consumer use, their ultimate fate will be strongly influenced by their interactions with microbial communities.[13–17] During the earliest stages of microbial exposure to CNTs that are present at a CNT/PNC surface, cell death has been observed with a number of different microorganisms such as *Escherichia coli* (*E. coli*), *Bacillus subtilus*, *Staphylococcus epidermidis* (*S. epidermidis*), and *Pseudomonas aeruginosa* (*P. aeruginosa*).[18–22] for *E. coli* and *P. aeruginosa*, it has been shown that this antimicrobial effect increases with mass fraction of CNTs (% w/w) at the surface, regardless of whether the CNTs are pristine, oxidized (O-CNT), multi-wall (MWCNT), or single-wall (SWCNT).[22,23] Mechanistic explanations of CNT cytotoxicity have been proposed that include cell membrane penetration by CNTs due to their high aspect ratio, cell membrane disruption, and oxidative stress.[21,24–29] While it has not been proved definitively which one or combination of these mechanisms is responsible for CNT cytotoxicity, it has been shown that cell death tends to occur only when CNTs are in direct contact with microorganisms, although not every single contact event necessarily leads to cell death.[22]

The initial interactions of microbes with CNT/PNCs can also potentially influence biofilm development, or the growth of microbial communities, at the CNT/PNC surface.[18,19,22,23] Biofilm formation begins with: (1) reversible cell attachment followed by, (2) cell division, (3) irreversible attachment using secreted extracellular polymeric substances (EPS), (4) maturation, and (5) cell dispersion to promote biofilm formation at other locales.[17,30,31] Biofilm formation occurs ubiquitously on most surfaces exposed to microbial populations and improves the tolerance of microorganisms to dry and/or nutrient deficient conditions, promotes nutrient accumulation from the environment, and keeps extracellular enzymes in close proximity to cells to aid in the metabolism of substrates.[32] Biofilms also play an important role in a wide range of environmental processes including the sieving, attachment to, or removal of contaminants from water; the stabilization of sediments; flocculation, settling, and dewatering in wastewater treatment; and biodegradation processes involving dissolved, colloidal, and solid organic materials such as oil droplets and polymeric materials.[32–34] For polymer surfaces that can be degraded by microorganisms, biofilm formation is also the prerequisite to biodegradation and the presence of CNTs could therefore influence the rate of this process.[35–37] In addition to their role in the natural environment, biofilms can decrease the efficiency of processes in industrial settings such as water flow in pipes and biofilms can lead to infections in the human body, oftentimes through formation on medical devices, where they have been shown to be 10–1000 times more resistant to antibiotics than planktonic cells.[16,30,38–45] Consequently, biofilm reduction and/or removal are commonly targeted by toxic release agents, low energy surfaces, and/or antimicrobial surfaces.[40,44–50]

CNTs are thought to have a physicochemical-dependent antimicrobial effect that derives from their ability to disrupt the formation of biofilms that develop on the surface of CNT/PNCs.[18–20,22,51] As a result efforts have been made to exploit the cytotoxicity of CNTs to create new anti-biofouling surfaces or improve existing anti-biofouling technologies.[18–21,43,52,53] For example, the use of CNT/PNCs as an antimicrobial surface coating has been proposed for SWCNTs dispersed into the biomedical polymer, poly(lactic-*co*-glycolic) acid (PLGA), which have been shown to significantly diminish the viability and metabolic activities of *E. coli* and *S. epidermidis* at the CNT/PNC surface.[21] CNT antimicrobial properties have also been exploited in water disinfection applications by modifying membranes with CNTs, although the long term biofilm growth on these surfaces has not been investigated.[43,54–56] To our knowledge, no studies have shown that CNT-containing surfaces can be used to detach microorganisms due solely to their antimicrobial properties. Instead, they have been used commercially in existing paints and coatings to further reduce marine organism growth on boat hulls by providing a nanostructured underlayer to a silicone or fluoropolymer surface with a low free energy of cell attachment.[44,45,52,53]

Since CNT/PNCs are expected to be one of the biggest projected commercial uses of CNTs, it is important to study the growth and development of biofilms on different types of CNT/PNC surfaces that will be present in the environment following consumer use.[4–8] In many cases, CNT/PNC products would be expected to have a buried CNT-structure or surface coating on which a biofilm would first grow. On the other hand, some CNT/PNCs might initially have CNTs exposed at the surface or CNTs that become exposed as a result of environmental degradation processes.[15,57–60] The effect of CNTs on mature biofilm growth has only been investigated or partially considered in a few studies.[43,51] In one study, Rodrigues and Elimelech determined that the antimicrobial properties of CNTs reduced biofilm growth on a CNT-coated surface over a 48 h time period but led to the release of nutrients from attached dead cells.[51] This release of nutrients was

hypothesized to promote biofilm colonization on top of the dead microbial layer which could serve as a protective barrier for living cells from the underlying, cytotoxic CNTs.[41,51] These "live-on-dead" biofilm structures have been observed in a biofilm development study on a silver–palladium antimicrobial surface, where cell death of a silver-resistant strain of *E. coli* occurred at the surface due to an electrochemical redox processes while silver-resistant microorganisms readily formed colonies atop this dead layer of cells.[61] "Live-on-dead" structures have also been observed in *Geobacter anodireducens* biofilms, grown on an electrode surface to form an active component in a bioelectrical system, under electrochemical conditions that were not conducive to maintaining a homogenous, metabolically active biofilm.[62] In contrast, a systematic study to analyze how biofilms develop on CNT/PNCs has not yet been investigated.

To address this question, the focus of the present study has been to compare and contrast biofilm growth on a range of different surfaces, including; (a) a polymer without CNTs, (b) PNC surfaces with different CNT loadings, where the CNTs were initially buried below the surface but became exposed as a result of polymer degradation during biofilm growth, and (c) a PNC surface where CNTs were initially exposed at the surface. To facilitate a comparison of these different scenarios, we used poly-ε-caprolactone (PCL) as a common polymer matrix. PCL was selected because it is benign to microorganisms and is commonly found in polymer blends used in trash bags, incontinence products, and bandage wrappers.[63] As a result, biofilm growth on PCL could be directly compared to biofilm growth on CNT/PNCs to clearly delineate any observed CNT effects from normal biofilm development processes.[38,39,64–68] PCL is also biodegradable, which allowed us to study how biofilm growth was impacted by the accumulation of CNTs at a polymer surface as a result of PCL biodegradation.[64–66,69] Oxidized multi-wall carbon nanotubes (O-MWCNTs) were chosen as the CNT filler since they were able to uniformly disperse within the PCL matrix and have previously been shown to exhibit cytotoxicity.[22] It should be noted that biodegradation of CNTs was not a factor in this study since this process has only been observed for oxidized CNTs exposed to harsh, acellular conditions involving enzymes such as horseradish peroxidase and even then, only partial biodegradation of O-MWCNTs was observed.[70,71]

Pseudomonas aeruginosa (*P. aeruginosa*) wild type was chosen as a model microorganism since *Pseudomonas* species readily form biofilms, are commonly found in the environment, and are able to biodegrade PCL.[64–66,69] For comparison of different aqueous environments, biofilms were grown under drip flow reactor (DFR) and static conditions, with and without low shear and constant replenishment of a food source, respectively.[72,73] Biofilm development on surfaces prepared with 0.5% and 2% w/w O-MWCNT/PCL, with the CNT loadings chosen for their commercial relevance, were monitored and compared at various growth stages to PCL (0% w/w O-MWCNTs) under the same conditions using LIVE/DEAD staining coupled to confocal laser scanning microscopy (CLSM).[9–12] This allowed us to differentiate green-fluorescent living cells from red-fluorescent dead cells based on membrane integrity.[74] Biomass and thickness analysis measurements were also made using COMSTAT 2 software to compare biofilm development on PCL *versus* CNT/PCL nanocomposites.[75,76]

Experimental

The experimental section is organized as follows: section I describes the preparation of CNT/PCL nanocomposites, section II describes the characterization of the prepared CNT/PCL nanocomposites, section III describes the methods and conditions used to grow biofilms on the CNT/PCL nanocomposite surfaces, and section IV describes how biofilm development was analyzed.

Section I: CNT/PCL nanocomposite preparation

Preparation of PCL and CNT/PCL casting solutions. Pristine MWCNTs (Nanocyl NC7000, outer diameter 9.5 nm, 1.5 μm length, 90% purity) were oxidized "in-house" to obtain O-MWCNTs with a total oxygen content of 4.1%, measured using X-ray photoelectron spectroscopy (XPS). Further information is provided in the ESI.† O-MWCNTs were also dispersed in 70 : 30 ethanol/water, sonicated for 30 s, and dried on a holey carbon grid for TEM characterization (JEOL JEM 1220, 120 kV accelerating voltage). From the TEM images, the O-MWCNT diameter distribution was measured in 15–20 areas using DigitalMicrograph software (Gatan Inc., Pleasanton, CA). The average O-MWCNT diameter was 9.4 ± 1.2 nm, consistent with the 9.5 nm diameter measured by the manufacturer. TEM data is shown in Fig. S1† along with XPS data on the atomic surface composition of the O-MWCNTs. O-MWCNTs were dispersed in chloroform (99.8% GR ACS, Cat #CX1055-6, EMD) to prepare two suspensions having concentrations of 50 mg L^{-1} (for 0.5% w/w O-MWCNT/PCL) and 200 mg L^{-1} (for 2% w/w O-MWCNT/PCL) O-MWCNTs. 1 g L^{-1} of ethyl cellulose (Sigma-Aldrich, Cat #433837), a natural and biocompatible surfactant, was added to each suspension to enhance the O-MWCNT colloidal stability in chloroform.[77,78] The O-MWCNT/ethyl cellulose suspensions were ultra-sonicated in a cold ice-water bath for 3 h (Branson 1510 bath sonicator, 70 watts) with the water changed every 20 min to avoid heating the suspension; these low temperatures optimized the CNT dispersion quality. 10 g L^{-1} poly-ε-caprolactone (PCL, Sigma-Aldrich, Cat #440752) was then added to each O-MWCNT/ethyl cellulose suspension to produce 0.5 or 2% w/w O-MWCNT/PCL casting solutions that were then ultra-sonicated for another 2 h following the same ice-water bath procedure. At this stage the suspensions were centrifuged (PowerSpin LX Centrifuge, Unico, USA) at 3000 rpm for 5 min to remove any glass or remaining bundled CNTs for a final concentration of slightly less than or equal to 50 or 200 mg mL^{-1} O-MWCNTs in the casting solution. Unmodified polymer without O-MWCNTs

was prepared by sonicating 10 g L^{-1} PCL in chloroform for 2 h with 1 g L^{-1} ethyl cellulose.

Preparation of PCL and CNT/PCL films suitable for CLSM imaging. Thin films of PCL and CNT/PCL nanocomposites were spray-coated onto modified glass microscope slides, since an underlying support is required for CLSM imaging. Due to the hydrophobicity of PCL, it was found that the glass slides required octadecyltrichlorosilane (OTS) modification to increase CNT/PCL nanocomposite adhesion (Fig. S2†).[79–83] Further information on OTS modification and characterization can be found in the ESI.† The spray-coating process, which is detailed in the ESI† and shown in Fig. S3,† yielded uniformly dark O-MWCNT/PCL coatings (0.5 and 2% w/w) as demonstrated in Fig. S2.†

Preparation of photolyzed CNT/PCL nanocomposites. Photodegraded samples were prepared by exposing CNT/PCL nanocomposites to hydroxyl radicals to mimic the effects of indirect photolysis in aqueous environments.[84–86] This represents a form of accelerated weathering. To generate these photodegraded CNT/PNC samples, thicker 2% w/w O-MWCNT/PCL nanocomposites, without an underlying OTS-modified slide, were prepared as described in the ESI.† CNT/PCL nanocomposites spray-coated onto OTS-modified glass slides were not used because initial studies revealed that photolysis caused some of the CNT/PCL coatings to detach into solution. As illustrated in Fig. S4,† photolysis was effected by tightly wrapping thick CNT/PCL samples around glass slides (4.0 cm × 1.2 cm × 0.1 cm) using Teflon tape and immersing these prepared samples individually into quartz test tubes (12.5 cm length, 1.3 cm diameter, Southern New England Ultraviolet Company, Branford, Connecticut) containing 0.5 M hydrogen peroxide solution.[86] The surfaces of these CNT/PCL samples were then exposed to both hydroxyl radicals and UV light by irradiating the hydrogen peroxide and immersed samples at 254 nm for 24 h at 35 °C in a Rayonet Photochemical Chamber Reactor (Model: RPR-100, Southern New England Ultraviolet Company, Branford, Connecticut, 1.62×10^{17} photons per s cm^{-3}, 16 bulbs).

Section II: CNT/PNC characterization

(i) Surface morphology and composition. Replicate SEM images of PCL, 2% w/w O-MWCNT/PCL, and 2% w/w O-MWCNT/polyvinyl alcohol (PVOH) nanocomposites are shown in Fig. S5–S7† and triplicate SEM images are shown for 0.5% w/w O-MWCNT/PCL nanocomposites in Fig. S8.† The preparation and analysis of replicate areas and separately prepared CNT/PNCs is further outlined in the ESI.† The 2% w/w O-MWCNT/PVOH nanocomposites were prepared by spray-coating and imaged using SEM to serve as a comparison to 2% w/w O-MWCNT/PCL nanocomposites as described in more detail in the ESI.† An SEM image of pure PVOH is provided for reference (Fig. S7†). In addition to the SEM image shown in Fig. 5, replicate SEM images (Fig. S9†) were also taken for 2% w/w O-MWCNT/PCL nanocomposites before and after photodegradation. Attempts were also made to image the surfaces of biodegraded CNT/PCL nanocomposites by removing the biofilm coating using 1% w/w sodium polyphosphate immersion for 5 days followed by rinsing with Milli-Q water, an example of which is shown in Fig. S10.†

(ii) PCL and CNT/PCL film thickness. Side-views of PCL and 2% w/w O-MWCNT/PCL coatings on OTS-modified slides were imaged in replicate areas (>5) using SEM. For each image, replicate thickness measurements (>5) of the PCL or 2% w/w O-MWCNT/PCL coating were made using ImageJ software (Bethesda, MD). Both PCL and 2% w/w O-MWCNT/PCL had a consistent thickness of approximately 1 μm across the OTS-modified slide.

Section III: Methods and conditions of biofilm growth on CNT/PCL surfaces

Inoculation of PCL and CNT/PCL surfaces. To begin a biofilm experiment, a 0.5 mL frozen culture of *P. aeruginosa* wild type (ATCC 27853) was added to 75 mL LB broth (25 g L^{-1}) and grown overnight to the stationary phase. on an incubator shaker at 225 rpm and 37 °C. The overnight cultures were grown in LB broth for rapid microbial growth which enabled practical timing in terms of transfer and growth in basal mineral media (BMM) followed by flow cell setup the next day. BMM was used for further growth and to match that of the sterile feed used in the DFR since it is well defined and more environmentally relevant.[87] Next, 0.20 mL of the overnight culture was transferred to 100 mL of BMM containing 3.270 g L^{-1} acetate and grown to the exponential phase (O.D. 0.040 to 0.060 at 540 nm) on the incubator shaker at 300 rpm. This corresponded to $3.0 \pm 0.1 \times 10^8$ CFU mL^{-1}, the average CFU mL^{-1} and standard deviation of two separately grown *P. aeruginosa* cultures. Further information on the *P. aeruginosa* frozen stocks and the BMM composition are provided in the ESI.†

In order to initiate biofilm growth under both static and drip flow conditions, PCL and CNT/PCL samples were first inoculated with 20 mL of the exponential phase *P. aeruginosa* culture for 1 h at room temperature. This allowed the *P. aeruginosa* to initially attach to the samples prior to biofilm development. Following initial *P. aeruginosa* attachment, a sterile BMM feed was flowed over the samples for the remainder of the experiments.

Drip flow reactor (DFR). The DFR used in this study was capable of housing six slides at one time for biofilm studies.[88] Immediately prior to an experiment, the DFR (Model DFR 11-6, BioSurface Inc., Bozeman, MT) was aseptically assembled and prepared according to the manufacturer's specifications. Modifications were made to meet our experimental needs (see Fig. S11†). Specifically, this involved setting the apparatus at a negative angle of −2.3° with the port side higher than the drip side, opposite to the ordinary DFR setting.[40,88,89] This allowed media to drip down the samples at a downward (positive) angle, facilitating complete sample immersion and a uniform media flow over the hydrophobic PCL and CNT/PCL samples. This prevented

inconsistent growth patterns and bacteria dry-out in different sample areas that would occur in the typical DFR configuration.

Biofilm experiments in the DFR were initiated by rinsing samples that had been inoculated for 1 h in depleted media (BMM with no acetate) to remove loosely adhered cells. Samples were then gently transferred into the DFR chambers, which were pre-filled with media to prevent drying. The media was then allowed to flow through 1.30 mm inner diameter tubing into each reactor chamber at a flow rate of 0.35 mL min^{-1}, corresponding to a flow residence time of 40 min, using an Ismatec BVK peristaltic pump (IDEX, Germany). This flow was sustained throughout the course of each experiment, which ranged in time from 6 to 96 h. Low carbon source (0.2 g L^{-1} acetate) BMM (low C BMM) was used since higher carbon source concentrations were found to cause additional biofilm formation at the air–liquid interface that hampered biofilm development on the samples, presumably as a result of oxygen depletion. The flow rate was checked before and after the experiment to ensure an approximate value of 0.35 mL min^{-1} was maintained; the flow rate was kept constant by using large inner diameter (8 mm) exit tubing to minimize fouling due to biofilm formation at the exit port. For every O-MWCNT/PCL nanocomposite placed in the DFR there was a corresponding PCL control. Four biofilm thickness regimes were identified based on the biofilm thicknesses measured on the PCL control.

Static experiments. After 1 h of initial microbial attachment, PCL and O-MWCNT/PCL nanocomposites were rinsed in depleted media to removed loosely attached microorganisms, and then transferred to sterile dishes containing 20 mL of low C BMM (0.2 g L^{-1} acetate) and sat for approximately 2 weeks under static conditions.

Photodegraded CNT/PCL nanocomposites were rinsed gently with sterile Milli-Q water five times and left tied to the glass slide for the inoculation procedure. Photodegraded CNT/PCL nanocomposites were inoculated under static conditions for 1 h and 2 weeks. The 2 week samples had 1 mL of BMM containing 3.270 g L^{-1} acetate added twice at regularly spaced intervals. This provided an additional food source sufficient to maintain microbial growth for the duration of the experiment.

Section IV: Analysis of biofilm development on CNT/PCL nanocomposites

LIVE/DEAD staining and confocal laser scanning microscopy (CLSM) imaging. At the end of an experiment, each sample was gently removed from the DFR chamber or dish used for static inoculation. Samples were then rinsed in depleted media (DM) to wash away any loosely adhered bacteria.[88] As outlined in the ESI,† a FilmTracer LIVE/DEAD Biofilm Viability Kit (Molecular Probes, Invitrogen) was used to differentiate the living and dead cells within the biofilms. Samples were then rinsed with depleted media to remove excess stain. LIVE/DEAD stained biofilms on the PCL and CNT/PCL surfaces were imaged using CLSM. Further information on image acquisition is detailed in the ESI.† Because the depth of field was too high to image biofilms within the DFR, biofilms were directly imaged using an inverted 40× water immersion objective, a method used previously to image LIVE/DEAD stained biofilms.[90,91] In this configuration, samples were coated with Vectashield Mounting Media (Vector Laboratories Inc., Burlingame, CA) to maintain fluorescence and prevent dryout that could interfere with the imaging results. Fluorescence intensity remained constant throughout the scanning of all biofilms, indicating that there were no photobleaching or quenching effects as a result of the CNTs, polymer, or the imaging conditions. Numerous staining procedural details were also followed to ensure the accuracy and validity of the results; these are outlined in our previous study and listed in the ESI.†[22] Additional background staining controls performed for the PCL and CNT/PCL samples used in this study are described in the ESI† and shown in Fig. S12 and S13.

Biofilm controls on glass slides and OTS-modified glass slides. Biofilms were grown on glass slides under both static (Fig. S14†) and drip flow conditions (Fig. S15†) for the longest exposures studied; 2 weeks and 72–96 h, respectively. They were then stained and imaged according to the protocol outlined in the previous section. Bacteria grown on OTS-modified slides for 6 h were also LIVE/DEAD stained and imaged to show that OTS was not cytotoxic (Fig. S16†).

Analysis of biofilm images. Three dimensional biofilm images (XYZ projections) were reconstructed by the microscope software Slidebook (Intelligent Imaging Innovations, Denver, CO). At least 6 replicate biofilm images were taken in different sample areas for every sample imaged. Replicate CLSM images are shown in Fig. S17–S21† for Fig. 2–5, respectively. Separately grown biofilms were also imaged (Fig. S17†) under DFR conditions to show consistency in biofilm development.

COMSTAT 2 biofilm analysis software was used to measure the biomass volume ($\mu m^3/\mu m^2$) and biomass thickness (μm) under both drip flow and static conditions for PCL and 2% w/w O-MWCNT/PCL nanocomposites (Fig. 2 and 4, Table S1†). These measurements were also made for 0.5% w/w O-MWCNT/PCL under DFR conditions.[75,76,92] As described in the ESI,† manual thickness measurements were also made to validate the COMSTAT 2 measurements and yielded similar results, as shown in Table S1.†

Results and discussion

The SEM images in Fig. 1 show the structure and morphology of: (a) PCL, (b) a 2% w/w O-MWCNT/PCL nanocomposite, and (c) a 2% w/w O-MWCNT/PVOH nanocomposite after spray-coating. A comparison of Fig. 1(a) and (b) reveals that the addition of CNTs to the PCL matrix leads to a rougher surface. Faint, but discernible CNT like structures are also observed in the 2% w/w O-MWCNT/PCL nanocomposite images. In contrast, SEM data for the 2% w/w O-MWCNT/PVOH

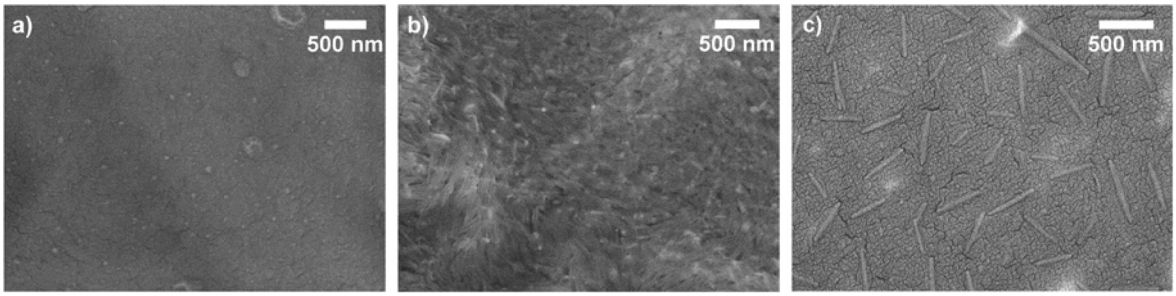

Fig. 1 SEM comparison of the surface morphology and CNT content of: a) PCL, b) 2% w/w O-MWCNT/PCL, and c) 2% w/w O-MWCNT/PVOH.

nanocomposite (Fig. 1c) shows clearly distinguishable CNT structures. It should be noted that the CNTs are somewhat broadened in diameter due to the presence of a platinum coating that was used to prevent charging during SEM.[22] Previous XPS studies have shown that CNTs present at the surface of PVOH are at a concentration representative of the CNT concentration (2% w/w) in the casting solution.[22] Although CNTs were not clearly distinguishable at the 2% w/w O-MWCNT/PCL nanocomposite surface, a uniformly dark PNC was produced, indicating the presence of well-distributed CNTs throughout the PCL matrix.[22] We interpret the difference in the SEM images between the CNT/PVOH

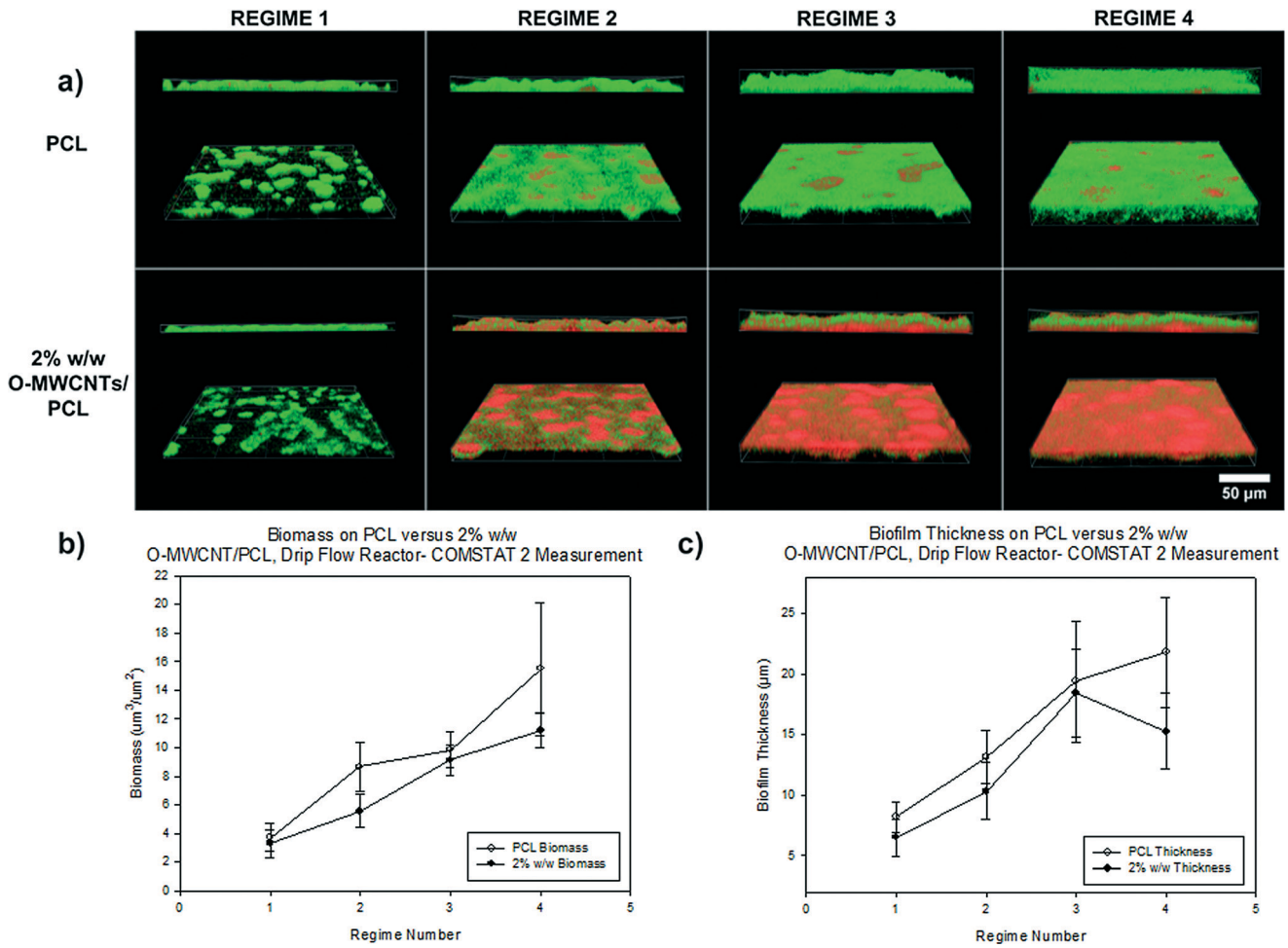

Fig. 2 a) CLSM images of LIVE/DEAD stained *P. aeruginosa* grown in a DFR on PCL (top row) and 2% w/w O-MWCNT/PCL (bottom row). Regimes 1–4 (6–96 h) represent increasing levels of biofilm growth based on the biofilm thicknesses observed on PCL. For each panel, the top image is a side view of the biofilm and the bottom image is the inverted biofilm to show where the biofilm makes contact with the sample surface. Quantitative comparison of biofilms on PCL and 2% w/w O-MWCNT/PCL under DFR conditions is also made using COMSTAT 2 b) biomass volume and c) thickness analysis. Each data point represents duplicate samples with at least five replicate areas per sample.

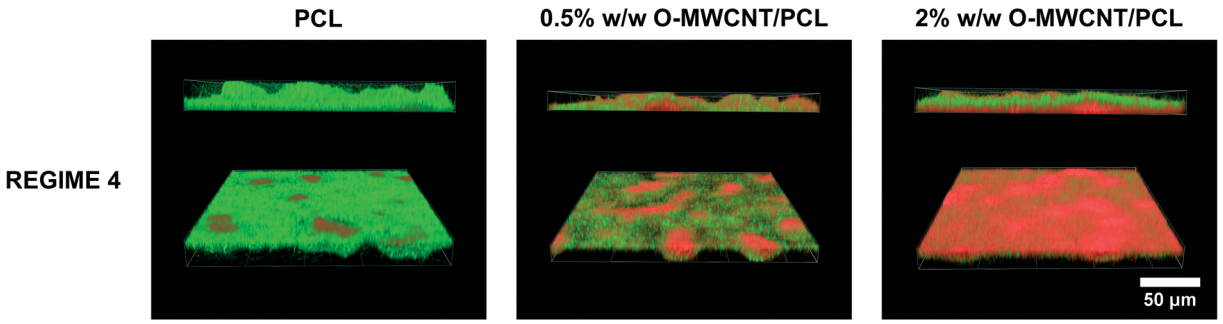

Fig. 3 A CLSM comparison of LIVE/DEAD stained *P. aeruginosa* biofilms grown in a DFR on PCL, 0.5% w/w, and 2% w/w O-MWCNT/PCL at regime 4.

and CNT/PCL nanocomposites to be an indication that the CNTs in the CNT/PCL nanocomposite are not present at the very topmost surface layer, but are slightly buried below the surface. This is also supported by the initially benign interaction of the microorganisms with the 2% w/w O-MWCNT/PCL nanocomposite, indicated by the green-fluorescent living cells

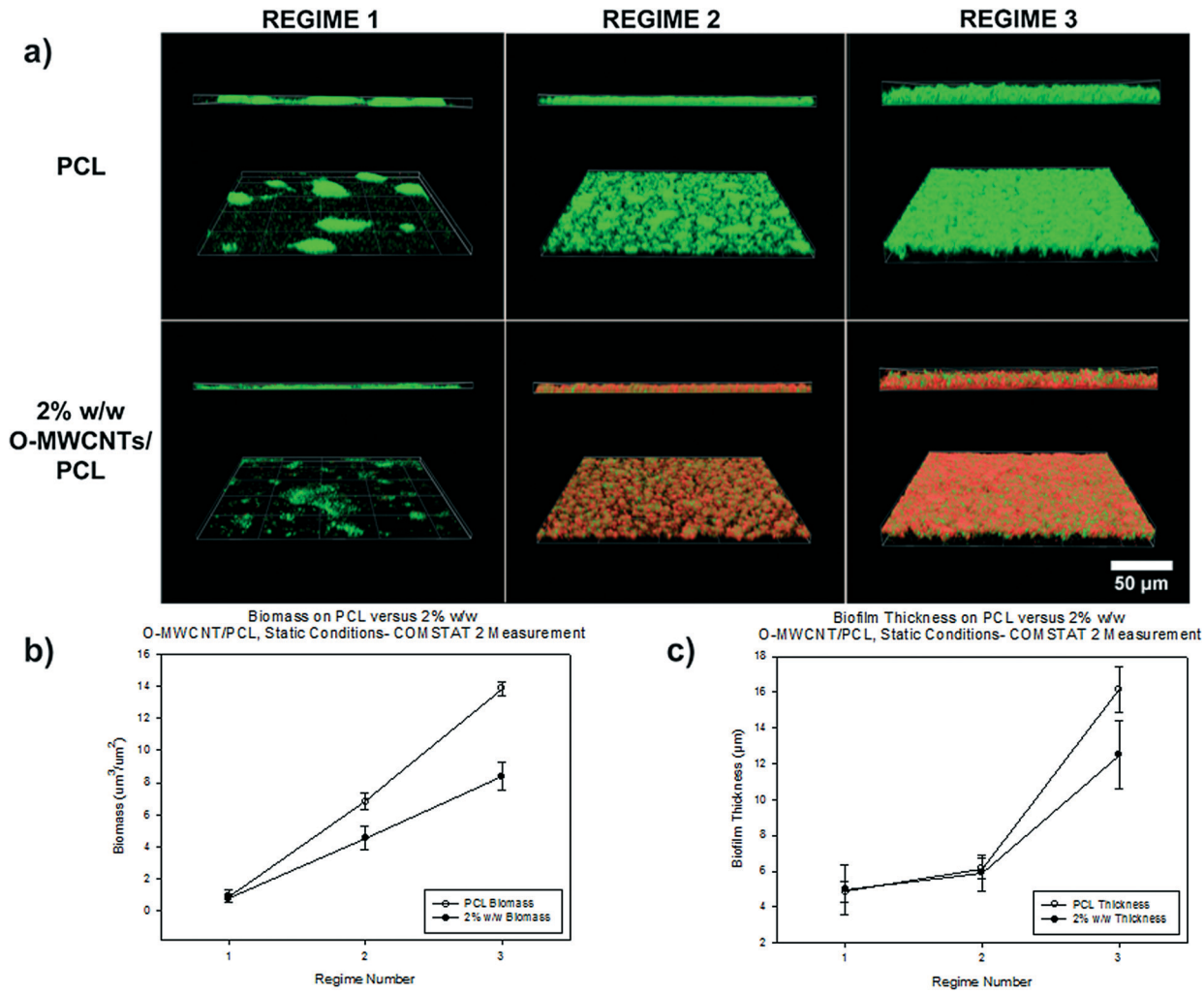

Fig. 4 a) CLSM images of LIVE/DEAD stained *P. aeruginosa* grown under static conditions on PCL (top row) and 2% w/w O-MWCNT/PCL (bottom row). Regimes 1–3 (1 h–2 weeks) represent increasing levels of biofilm growth based on the biofilm thicknesses observed on PCL. Quantitative comparison of biofilms on PCL and 2% w/w O-MWCNT/PCL under static conditions is also made using COMSTAT 2 b) biomass volume and c) thickness analysis. Each data point represents duplicate samples with at least five replicate areas per sample.

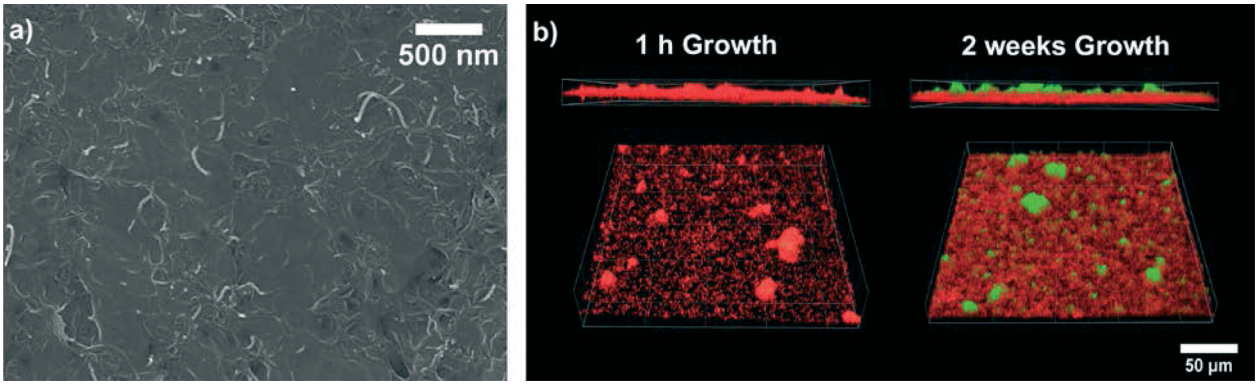

Fig. 5 a) An SEM image showing CNT accumulation at the surface of a 2% w/w O-MWCNT/PCL nanocomposite following exposure to H_2O_2 in the presence of UV irradiation for 24 h and b) CLSM images of LIVE/DEAD stained *P. aeruginosa* grown on this type of photolyzed surface under static conditions for 1 h and 2 weeks with acetate food source replenishment.

in the bottom left panel of Fig. 2a, which is in sharp contrast to the cytotoxicity of the CNT/PVOH nanocomposites at similar CNT mass fractions in our previous study.[22] Buried-CNT structures have been observed previously with CNT/PNCs such as MWCNT/epoxy while in other cases, CNTs have been shown to reside at the surface or accumulate gradually during environmental degradation processes.[15,22,23,57,93]

Fig. 2a shows the progression of *P. aeruginosa* biofilm growth on PCL (top panels) and 2% w/w O-MWCNT/PCL (bottom panels) surfaces. Since *P. aeruginosa* can biodegrade PCL but not CNTs, our hypothesis was that the CNT/PCL surface characteristics would transform, and that these changes would influence biofilm development. The top CLSM image within each panel (*e.g.* PCL regime 1) is a side view of the biofilm while the bottom image is inverted to show the part of the biofilm in direct contact with the surface. In these experiments *P. aeruginosa* biofilms were grown on PCL and 2% w/w O-MWCNT/PCL surfaces in a DFR. The DFR was used to simulate slow-flowing water in the environment (~200 mL h^{-1}) such as freshwater rivers and thermal hot springs.[72] In these experiments, the biofilm thicknesses on PCL samples were used as a point of reference to track the maturity of the biofilms on the CNT/PCL nanocomposites. The use of the PCL samples as an internal reference was found to be necessary as precise time-course evolution between different *P. aeruginosa* cultures was too variable. Based on this approach, the maturity levels of the biofilms were classed into four regimes based on the biofilm thickness observed on the PCL surface (measured as an average of ≥6 images with COMSTAT 2): the primary (regime 1), secondary (regime 2), tertiary (regime 3) and final (regime 4) stage with biofilm thicknesses of 8 ± 1 μm, 13 ± 2 μm, 19 ± 5 μm, and 22 ± 5 μm, respectively (Fig. 2c). Biomass volume measurements also increased on PCL between each regime as shown in Fig. 2b and Table S1.†

During the initial period of biofilm growth (regime 1) the CLSM images show discrete colonies formed on both PCL and 2% w/w O-MWCNT/PCL surfaces, dominated almost exclusively by living cells. Indeed, the structure of the biofilms that initially form on the two surfaces are similar in terms of a high number of green-fluorescent, living cells with a slight difference in terms of thickness (8 ± 1 μm for PCL *versus* 7 ± 1 μm for 2% w/w O-MWCNTs). The initially benign interaction of microorganisms with the nanocomposite surface is further supported by Fig. S22† which shows green-fluorescent, living cells on the 2% w/w O-MWCNT/PCL surface from 1 h of initial attachment to 6 h of static microbial growth. In our previous study O-MWCNTs were shown to be cytotoxic towards *P. aeruginosa*. Consequently, the initially benign nature of the 2% w/w O-MWCNT/PCL surface is consistent with the lack of CNTs at the PNC surface as suggested by the SEM data in Fig. 1(b). The absence of initial cytotoxicity for the CNT/PCL nanocomposite surface is also a reflection of the need for direct contact to occur between CNTs and microorganisms for the antimicrobial effect of CNTs to become operative.[22]

In regime 2, however, differences begin to appear in the nature of the biofilms on the two surfaces. For PCL, the thickness of the biofilm increases (8 ± 1 μm to 13 ± 2 μm) as the surface becomes uniformly covered with *P. aeruginosa*. Although the vast majority of the attached cells are green-fluorescent, living cells, a small number of dead cells (red-fluorescent) are now observed at the interface between the PCL surface and the biofilm. These red-fluorescent dead cells are localized inside the mushroom-like colonies, consistent with the natural biofilm development process in which dead cells appear deep within the biofilm because they are used as an additional food source or aid in biofilm sloughing.[38,39,67,68] On the 2% w/w O-MWCNT/PCL nanocomposite, the biofilm thickness also increases between regimes 1 and 2 (7 ± 1 μm to 10 ± 2 μm) although it remains thinner than the biofilm formed on the PCL. However, the most striking difference in the biofilms on the PCL and O-MWCNT/PCL surfaces is the distribution of living and dead cells. Specifically, the biofilm on the 2% w/w O-MWCNT/PCL surface in regime 2 is now dominated by red (dead) cells in direct contact with the surface, although some green (living) cells are still observed. We attribute this marked change in the properties of the 2%

w/w O-MWCNT/PCL nanocomposite between regime 1 and 2 to biodegradation of the PCL polymer, leading to exposure of CNTs at the surface and the onset of cytotoxicity. The delayed onset of cytotoxicity at the 2% w/w O-MWCNT/PCL surface is consistent with the idea that the CNTs were initially present below the nascent PNC surface prior to biodegradation (see Fig. 1(b)).

PCL biodegradation has been observed before by biofilms used in denitrification applications and with *P. aeruginosa* in mass loss studies conducted in our laboratory.[94] In this study, only a thin (nanometer scale) thickness of the PCL coating is required to expose CNTs at the surface by PCL biodegradation. Although we could not directly measure PCL biodegradation on the 1 μm thick CNT/PNC film used in this study, we have performed related studies where mg quantities of pure PCL are degraded by *P. aeruginosa* cultures over the course of a few months. In contrast, we have seen no evidence that *P. aeruginosa* can biodegrade CNTs or the ethyl cellulose surfactant over a similar timescale. Thus, all of the experimental evidence points to the accumulation of CNTs at the surface being a result of PCL biodegradation.

It should be noted that the cytotoxicity of the CNTs in the present study is observed despite the fact that the CNT surfaces are oxidized and presumably at least partially coated with the surfactant ethyl cellulose. In our previous study, we have confirmed that oxidized MWCNTs and SWCNTs can exhibit antimicrobial properties at the surface of CNT/PNCs.[22] In this case, the addition of ethyl cellulose clearly does not mitigate the cytotoxicity of the O-MWCNTs as well. Ethyl cellulose itself does not contribute to the cytotoxicity since it is known to be biocompatible and is also present in the unmodified polymer references on which active biofilm growth occured.[76,77] Collectively, these observations suggest that different CNTs embedded in PNC materials will display cytotoxicity regardless of CNT type, surface oxidation, or the presence of a surfactant.[22,23]

By the tertiary stage of growth, differences between the biofilms on the PCL and 2% w/w O-MWCNT/PCL surfaces are even more dramatic. While the bacteria at the PCL/biofilm interface are still composed almost exclusively of living cells with the exception of some dead cells in the thicker biofilm regions, the 2% w/w O-MWCNT/PCL surface is now best described as a carpet of dead cells at the PNC/biofilm interface. Relative to regime 2, the increase in cytotoxicity of the 2% w/w O-MWCNT/PCL surface for regime 3 can be explained by the continued biodegradation of the PCL polymer, leading to a continuously increasing concentration of CNTs at the PNC/biofilm interface and a correspondingly more cytotoxic surface. In general, the appearance of the PNC/biofilm interface for regime 4 was similar to regime 3 with slightly more dead cells carpeting the surface of the CNT/PNC. One possible explanation for the cell death observed in the lower layers of the biofilm is that the CNTs are simply blocking access of the microorganisms to the underlying PCL substrate, which is serving as a food source. This possibility was ruled out by conducting separate control studies where biofilms were grown on glass slides to similar thicknesses (>20 μm) as those observed in regime 4. These studies revealed that the acetate and oxygen concentrations in the media were sufficient to keep the majority of the biofilm cells alive on an inert, glass surface (Fig. S15†). Consequently, the cell death observed on 2% w/w O-MWCNT/PCL nanocomposites can be reasonably attributed to antimicrobial contact between *P. aeruginosa* and CNTs.

In addition to the carpet of dead cells at the PNC/biofilm interface, the CLSM images in Fig. 2a (regime 3) reveal the presence of a layer of living (green) cells on top of the dead layer. This observation is indicative of the ability of a metabolically active biofilm to form on top of a dead layer, the latter acting to effectively shield the living cells from the cytotoxicity of the CNTs.[41,51] Upon moving from regime 2 to regime 3, the biofilm thickness increases on both the PCL (13 ± 2 μm to 19 ± 5 μm) and the 2% w/w O-MWCNT/PCL nanocomposite (10 ± 1 μm to 18 ± 4 μm), despite the differences in cytotoxicity between the two surfaces.

Transitioning from regime 3 to 4, the biofilm thickness increases on the PCL surface (19 ± 5 μm to 22 ± 5 μm) while the biofilm thickness on the 2% w/w O-MWCNT/PCL nanocomposite decreases slightly (18 ± 4 μm to 15 ± 3 μm). However, on the 2% w/w O-MWCNT/PCL nanocomposite, biomass volume (>20%) increases from regime 3 to 4. This indicates further microbial growth despite a compression in biofilm thickness, possibly a result of living microorganisms consuming cellular material from the underlying dead layer of microorganisms.[51] Overall, the same type of "live-on-dead" biofilm structure observed in regime 3 is also present in regime 4 on the 2% w/w O-MWCNT/PCL nanocomposite.

A schematic representation of biofilm development on PCL and 2% w/w O-MWCNT/PCL nanocomposites from regimes 1 to 4 is shown in Fig. 6a and b, respectively, highlighting the increase in cytotoxicity of the CNT/PCL surface due to

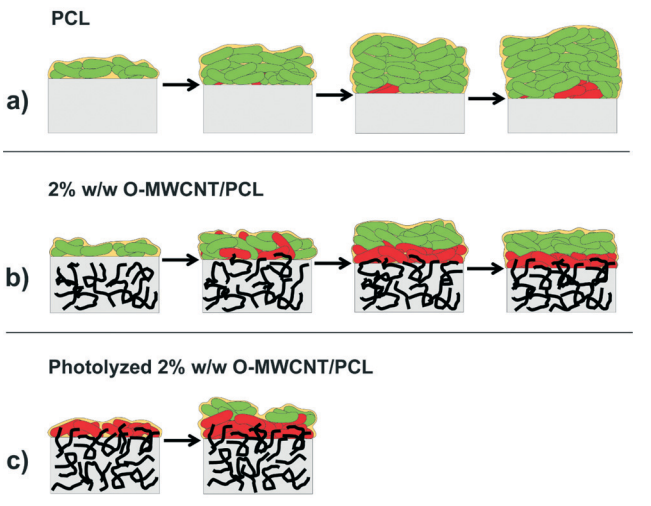

Fig. 6 Illustrations that compare biofilm development on a) PCL and b) 2% w/w O-MWCNT/PCL, transformed as a result of polymer biodegradation under DFR conditions, and on c) photolyzed 2% w/w O-MWCNT/PCL with CNTs initially present at the CNT/PNC surface.

the accumulation of CNTs as a result of PCL biodegradation and the subsequent formation of a "live-on-dead layer." This "live on dead" phenomenon is consistent with our previous study, where even at very short time points (1 h) on initially CNT-covered surfaces, some living bacteria were shielded by a layer of dead bacteria in direct contact with the underlying CNTs. It should be noted that biofilm formation will also be accompanied by the secretion of EPS which contributes to the increase in biomass volume. Although we did not stain specifically for EPS, the EPS produced during biofilm growth did not prevent the onset of CNT cytotoxicity as indicated by the formation of a dead cell layer in Fig. 2a. Accounting for the vertical resolution and fluorescence scattering between optical slices discussed in our previous publication, we estimate that this dead layer corresponds to a layer of one to three microorganisms (2–7 μm thick), consistent with the need for direct contact to occur in order for CNTs to exert their cytotoxicity.[22]

DFR experiments and biofilm analysis were also performed after initial attachment and at the final growth stage (regime 4) on an O-MWCNT/PCL nanocomposite with a lower (0.5% w/w) CNT concentration. CLSM images of LIVE/DEAD stained *P. aeruginosa* after 1 h of attachment to 0.5% w/w O-MWCNT/PCL nanocomposites (Fig. S23†) show that the CNT/PCL surface is initially benign. This is consistent with the absence of CNTs or a low CNT loading at the surface, the latter suggested by the SEM images (Fig. S8†). At regime 4 of biofilm development, or the final growth stage (Fig. 3(b)), the 0.5% w/w O-MWCNT/PCL nanocomposite surface contains a mixture of living and dead cells, somewhere intermediate between the fraction of dead cells on the PCL control shown in Fig. 3(a) and the 2% w/w O-MWCNT/PCL nanocomposite shown in Fig. 3(c). Thus, for the 0.5% w/w O-MWCNT/PCL nanocomposite it appears that the accumulation of CNTs from polymer biodegradation has not yet reached a point where the concentration of CNTs exposed at the surface is sufficient to have a cytotoxic effect on all of the attached *P. aeruginosa*. This implies that the rate at which a biofilm forms a dead layer of cells would vary with CNT loading as the surface degrades. COMSTAT analysis also reveals that the biofilm thickness (and biomass volume) on the 0.5% O-MWCNT/PCL nanocomposite is less than on the PCL (15 ± 1 μm *versus* 22 ± 3 μm). In contrast, the biofilm thickness on the 0.5% w/w is similar to the biofilm thickness on the 2% w/w O-MWCNT/PCL nanocomposite (15 ± 1 μm *versus* 15 ± 3 μm) despite the significantly larger fraction of dead cells on the 2% w/w O-MWCNT/PCL nanocomposite.

To compare the effect of growth conditions, biofilms were grown on PCL and 2% w/w O-MWCNT/PCL nanocomposites under static conditions without shear or food source replenishment. In contrast to the DFR, static conditions simulate another type of environmentally relevant setting involving microbial growth in stagnant water such as puddles, swamps, slow moving groundwater, or small ponds.[73] In these experiments, biofilm development was monitored on O-MWCNT/PCL nanocomposites at three stages, each corresponding to an increasing biofilm thickness on PCL reference samples. A comparison of drip flow (Fig. 2a) and static conditions (Fig. 4a) reveals that the biofilms grown under static conditions differ in terms of morphology. Specifically, the biofilm structure is much more uniform under static conditions because growth is not influenced by flow currents. This is most evident by the mushroom-like colonies and heterogeneous biofilms formed in the DFR.[72,88] However, both drip flow and static conditions produce similar biofilm growth patterns on PCL and 2% w/w O-MWCNT/PCL surfaces (compare Fig. 2 and 4). Under both growth conditions, the initial biofilms on PCL and 2% w/w O-MWCNT/PCL surfaces consist of mostly living cells, the green-fluorescent biofilm becomes thicker on the PCL control, and a red-fluorescent dead layer of cells eventually forms at the 2% w/w O-MWCNT/PCL nanocomposite/biofilm interface (Fig. 2a and 4a). Additionally, for the 2% w/w O-MWCNT/PCL nanocomposites, green-fluorescent living cells are observed on top of dead cells in the later stages of biofilm development (Fig. 2a and 4a, regime 3). For the same samples, similar biofilm development trends were observed in terms of changes in biofilm thickness and biomass volumes under both static and DFR conditions (summarized in Fig. 2b, c, 4b and c, and Table S1†). The absolute values of biofilm thickness and biomass volume were generally lower on CNT/PCL nanocomposites than on the pure polymer, presumably because CNT accumulation from polymer degradation led to cell death. However, biofilm thickness and biomass volume still increased at each stage of biofilm development as a result of active biofilm growth that continued on top of a dead layer of cells.

It is also worth noting that although both DFR and static conditions produce a "live-on-dead" biofilm structure, a much thicker layer of green-fluorescent living cells atop a carpet of dead cells is observed for the DFR biofilm than for the static biofilm. We ascribe this difference to carbon source depletion that limits cell growth under static conditions (Fig. 4) and carbon source replenishment under DFR conditions that promotes cell division at the surface. Rapid cell division as a result of the continuous carbon source feed can also account for the similarities in the biofilm thickness and volume on both 0.5 and 2% w/w O-MWCNT/PCL under DFR conditions (Fig. 3). Regardless, under both growth conditions a dead cell layer was required to allow living cells to grow on top of the CNT surfaces, as illustrated in Fig. 6b (DFR conditions) and Fig. S24† (static conditions). Under both flow and static conditions, the antimicrobial effect of CNTs on biofilm formation could be clearly observed over time as the CNTs accumulated at the PNC/biofilm interface due to biodegradation of the surrounding polymer matrix.[64–66] However, attempts were made to remove the biofilm without success by immersing samples in a 2% w/w sodium polyphosphate solution for 48 h with and without shaking followed by several washes with the same solution; this preventing us from directly observing CNTs at the CNT/PNC surface following polymer biodegradation (with SEM).[95,96]

To study the biofilm formation characteristics of a CNT/PNC where CNTs were initially present at the surface, static

biofilms were grown on 2% w/w O-MWCNT/PCL nanocomposites that were first degraded under aggressive oxidizing conditions (Fig. 5). This was carried out by exposing O-MWCNT/PCL nanocomposites to H_2O_2 in the presence of UV irradiation for 24 h. SEM analysis shown in Fig. 5 reveals that this treatment causes the removal of a thin layer of PNC and the accumulation of a large concentration of CNTs at the surface (2.1% average mass loss). Studying biofilm growth on this type of surface was also motivated by the expectation that many PNC surfaces will accumulate CNTs at the PNC/air interface over time as a result of naturally occurring environmental degradation processes such as photolysis and weathering.[15,57,59,60] As shown in Fig. 5, after 1 h of *P. aeruginosa* inoculation, almost all of the cells that attached to this type of CNT/PNC surface experienced cell death. This is in marked contrast to the initially benign surfaces observed for the 2% w/w O-MWCNT/PCL nanocomposites that had not been photolyzed (compare Fig. 4a, regime 1 and Fig. 5b). However, after 2 weeks of growth under static conditions with the acetate food source replenished twice, "live-on-dead" structures were observed. Results from these studies further support the idea that a CNT-covered surface leads to cell death for bacteria that come into direct contact with the CNTs but not for those protected by a conditioning layer of dead cells.

Overall, "live-on-dead" biofilm structures formed on all CNT/PCL surfaces once coated by a full dead layer of cells under both static and DFR conditions. This was in stark contrast to the green-fluorescent biofilms formed on PCL. To highlight biofilm development on CNT/PNCs with different surface characteristics, a side-by-side comparison of biofilm progression is illustrated for: (a) pure PCL, (b) 2% w/w O-MWCNT/PCL nanocomposites that accumulate CNTs at the surface during polymer biodegradation, and (c) and 2% w/w O-MWCNT/PCL nanocomposites that have CNTs initially present at the surface (Fig. 6). We assert that the biofilm development process observed on CNT/PCL nanocomposites in this study can be generalized to other types of polymer matrices. Fig. 6c represents how biofilms would develop on CNT/PNCs where CNTs are initially present at the surface, or CNT/PNCs where CNTs have accumulated as result of weathering (*e.g.* photolysis, wear) prior to microbial interaction, while Fig. 6b would be appropriate for CNT/PNCs in contact with microorganisms as CNTs accumulate at the PNC surface over time during environmental transformation processes (*e.g.* biodegradation, dissolution, *etc.*).[15,57–60]

Our results reinforce the hypothesis that CNT/PNC surfaces are only cytotoxic until they become coated with dead bacteria, limiting their use as antimicrobial materials. This conditioning layer of dead cells has been observed on other surfaces such as Ag–Pd and can be considered an inherent weakness of many anti-biofouling technologies that use solely cytotoxic effects to combat biofilm growth.[61] However, further studies on the stability of this "live-on-dead" biofilm structure will be useful to assess if there are conditions under which this type of biofilm sloughs away, allowing biofilms to form and subsequently be released in cycles on CNT/PNC surfaces. If biofilms are able to detach from CNT/PNCs, this would improve the potential for CNT/PNC surfaces to be used as antimicrobial coatings, at least in certain situations.

The dead layer of bacteria observed on CNT/PNCs also has the potential to affect the biodegradation of the underlying polymer matrix, a process in which extracellular enzymes produced by the attached microbial community can use the polymer substrate as a food source and break down polymeric chains to lower molecular weight units and eventually to small molecules such as CO_2 and water.[15,35–37,57,59,60,97–103] Since CNT accumulation can lead to a full layer of dead cells across the CNT/PNC surface but living cells can form on top of the dead cells, the living cells may still be able to metabolize the PCL substrate using the EPS of the biofilm matrix. However, the dead cell layer may instead serve as a barrier that prevents living cells from accessing and biodegrading the underlying PCL. Therefore it is unclear whether the full dead layer of cells formed as a result of CNT accumulation will render the CNT/PNC persistent or allow for continued biodegradation of the polymer matrix.

Conclusions

This study provides insights into how the development of biofilms on CNT/PNCs will be influenced by the surface characteristics of the CNT/PNC. The CNT/PCL nanocomposites studied had an initially benign interaction with microorganisms due to the lack of CNTs present at the surface. However, as the PCL matrix biodegraded, enrichment of CNTs at the surface increased the surface cytotoxicity. In terms of CNT loading, a dead cell layer was formed on the 2% w/w O-MWCNT/PCL nanocomposite but not on the 0.5% w/w O-MWCNT/PCL nanocomposite, indicating that CNT loading will have an effect on the rate at which the CNT/PNC surface becomes antimicrobial. On CNT/PCL samples where CNTs were initially exposed at the surface to simulate a weathered CNT/PCL nanocomposite, a full dead layer of cells was observed. At each growth stage, biofilm thickness and biofilm volume were always lower on CNT/PCL surfaces as compared to PCL. Since direct contact between the microorganisms and the CNTs was required for cell death, active biofilm growth occurred on all CNT-containing surfaces once a full layer of dead cells had formed at the PNC/biofilm interface. This demonstrates that once CNT/PNCs with a buried CNT network accumulate CNTs as a result of environmental transformation, the formation of a "live-on-dead" biofilm structure will be similar to that observed on CNT/PNCs with CNTs already present at the surface. The pattern of biofilm development was found to be similar under both DFR and static conditions although the rate of biofilm formation and structure of the biofilm differed. Collectively, the results of this study have implications for the fate and persistence of CNT/PNC products in the environment and the likely limitations of CNT/PNCs in anti-biofouling applications.

Acknowledgements

The authors would like to thank the NSF (CBET #1236493). DGG also acknowledges the DGG also acknowledges the Owens Graduate Fellowship awarded by the Johns Hopkins University Chemistry Department. The authors would like to thank Kris Marsh and Julianne Payne for their contributions as well as Dr. Michael McCaffery and Erin Pryce of the Integrated Imaging Center for their guidance in image acquisition and processing. Cong Gao acknowledges the Chinese Scholarship Council (No. 201406170083) for support to take part in this project.

References

1 N. G. McCrum, C. P. Buckley and C. B. Bucknall, *Principles of polymer engineering*, Oxford University Press, New York, 1997.
2 P. C. A. M. M. C. Painter, *Fundamentals of polymer science: an introductory text*, Technomic Pub. Co., Lancaster, PA, 1997.
3 G. Williams, R. Trask and I. Bond, *Composites, Part A*, 2007, **38**, 1525–1532.
4 C. McClory, S. J. Chin and T. McNally, *Aust. J. Chem.*, 2009, **62**, 762–785.
5 A. M. K. Esawi and M. M. Farag, *Mater. Des.*, 2007, **28**, 2394–2401.
6 M. H. Rahmat and P. Hubert, *Compos. Sci. Technol.*, 2011, **72**, 72–84.
7 R. Gangopadhyay and A. De, *Chem. Mater.*, 2000, **12**, 608–622.
8 M. Moniruzzaman and K. I. Winey, *Macromolecules*, 2006, **39**, 5194–5205.
9 (WWICS), Woodrow Wilson International Center for Scholars, "*The Project on Emerging Nanotechnologies*" *Nanotechnology Consumer Products Inventory*, http://www.nanotechproject.org/inventories/consumer/.
10 T. V. Duncan, *J. Colloid Interface Sci.*, 2011, **363**, 1–24.
11 *Nanocyl, Carbon nanotube applications: fuel system components:*, http://www.nanocyl.com/Products-Solutions/Sectors/Automotive/Fuel-System-Components.
12 V. M. F. L. De, S. H. Tawfick, R. H. Baughman and A. J. Hart, *Science*, 2013, **339**, 535–539.
13 E. J. Petersen, L. W. Zhang, N. T. Mattison, D. M. O'Carroll, A. J. Whelton, N. Uddin, T. Nguyen, Q. G. Huang, T. B. Henry, R. D. Holbrook and K. L. Chen, *Environ. Sci. Technol.*, 2011, **45**, 9837–9856.
14 S. Hirth, L. Cena, G. Cox, Ž. Tomović, T. Peters and W. Wohlleben, *J. Nanopart. Res.*, 2013, **15**, 1–15.
15 C. Kingston, R. Zepp, A. Andrady, D. Boverhof, R. Fehir, D. Hawkins, J. Roberts, P. Sayre, B. Shelton, Y. Sultan, V. Vejins and W. Wohlleben, *Carbon*, 2014, **68**, 33–57.
16 P. R. Jones, M. T. Cottrell, D. L. Kirchman and S. C. Dexter, *Microb. Ecol.*, 2007, **53**, 153–162.
17 J. W. Costerton, K. J. Cheng, G. G. Geesey, T. I. Ladd, J. C. Nickel, M. Dasgupta and T. J. Marrie, *Annu. Rev. Microbiol.*, 1987, **41**, 435–464.
18 F. Ahmed, C. M. Santos, R. A. M. V. Vergara, M. C. R. Tria, R. Advincula and D. F. Rodrigues, *Environ. Sci. Technol.*, 2012, **46**, 1804–1810.
19 C. M. Santos, K. Milagros Cui, F. Ahmed, M. C. R. Tria, R. A. M. V. Vergara, A. C. de Leon, R. C. Advincula and D. F. Rodrigues, *Macromol. Mater. Eng.*, 2012, **297**, 807–813.
20 M. S. Mauter and M. Elimelech, *Environ. Sci. Technol.*, 2008, **42**, 5843–5859.
21 S. Aslan, C. Z. Loebick, S. Kang, M. Elimelech, L. D. Pfefferle and T. P. R. Van, *Nanoscale*, 2010, **2**, 1789–1794.
22 D. G. Goodwin, K. M. Marsh, I. B. Sosa, J. B. Payne, J. M. Gorham, E. J. Bouwer and D. H. Fairbrother, *Environ. Sci. Technol.*, 2015, **49**, 5484–5492.
23 J. D. Schiffman and M. Elimelech, *ACS Appl. Mater. Interfaces*, 2011, **3**, 462–468.
24 S. Kang, M. Herzberg, D. F. Rodrigues and M. Elimelech, *Langmuir*, 2008, **24**, 6409–6413.
25 S. Kang, M. Pinault, L. D. Pfefferle and M. Elimelech, *Langmuir*, 2007, **23**, 8670–8673.
26 C. D. Vecitis, K. R. Zodrow, S. Kang and M. Elimelech, *ACS Nano*, 2010, **4**, 5471–5479.
27 L. M. Pasquini, R. C. Sekol, A. D. Taylor, L. D. Pfefferle and J. B. Zimmerman, *Environ. Sci. Technol.*, 2013, **47**, 8775–8783.
28 L. M. Pasquini, S. M. Hashmi, T. J. Sommer, M. Elimelech and J. B. Zimmerman, *Environ. Sci. Technol.*, 2012, **46**, 6297–6305.
29 C. Yang, J. Mamouni, Y. Tang and L. Yang, *Langmuir*, 2010, **26**, 16013–16019.
30 D. Monroe, *PLoS Biol.*, 2007, **5**, e307.
31 S. Andersson, G. K. Rajarao, C. J. Land and G. Dalhammar, *FEMS Microbiol. Lett.*, 2008, **283**, 83–90.
32 H.-C. Flemming and J. Wingender, *Nat. Rev. Microbiol.*, 2010, **8**, 623–633.
33 S. U. Gerbersdorf, T. Jancke, B. Westrich and D. M. Paterson, *Geobiology*, 2008, **6**, 57–69.
34 M. M. Klausen, T. R. Thomsen, J. L. Nielsen, L. H. Mikkelsen and P. H. Nielsen, *FEMS Microbiol. Ecol.*, 2004, **50**, 123–132.
35 A. Sivan, *Curr. Opin. Biotechnol.*, 2011, **22**, 422–426.
36 L. V. Evans, *Biofilms: recent advances in their study and control*, CRC press, 2003.
37 J. D. Bryers, *Biofilms II: process analysis and applications*, Wiley-Liss, 2000.
38 L. Ma, M. Conover, H. Lu, M. R. Parsek, K. Bayles and D. J. Wozniak, *PLoS Pathog.*, 2009, **5**, e1000354.
39 J. S. Webb, L. S. Thompson, S. James, T. Charlton, T. Tolker-Nielsen, B. Koch, M. Givskov and S. Kjelleberg, *J. Bacteriol.*, 2003, **185**, 4585–4592.
40 R. P. Carlson, R. Taffs, W. M. Davison and P. S. Stewart, *J. Biomater. Sci., Polym. Ed.*, 2008, **19**, 1035–1046.
41 H.-C. Flemming, T. Griebe and G. Schaule, *Water Sci. Technol.*, 1996, **34**, 517–524.
42 N. Billings, M. M. Ramirez, M. Caldara, R. Rusconi, Y. Tarasova, R. Stocker and K. Ribbeck, *PLoS Pathog.*, 2013, **9**, e1003526.

43 V. K. K. Upadhyayula and V. Gadhamshetty, *Biotechnol. Adv.*, 2010, **28**, 802–816.
44 S. Cao, J. Wang, H. Chen and D. Chen, *Chin. Sci. Bull.*, 2011, **56**, 598–612.
45 S. Krishnan, C. J. Weinman and C. K. Ober, *J. Mater. Chem.*, 2008, **18**, 3405–3413.
46 A. K. Epstein, T.-S. Wong, R. A. Belisle, E. M. Boggs and J. Aizenberg, *Proc. Natl. Acad. Sci. U. S. A.*, 2012, **109**, 13182–13187.
47 I. Francolini, P. Norris, A. Piozzi, G. Donelli and P. Stoodley, *Antimicrob. Agents Chemother.*, 2004, **48**, 4360–4365.
48 M. Ratova and A. Mills, *J. Photochem. Photobiol., A*, 2015, **299**, 159–165.
49 X. Khoo, G. A. O'Toole, S. A. Nair, B. D. Snyder, D. J. Kenan and M. W. Grinstaff, *Biomaterials*, 2010, **31**, 9285–9292.
50 C. Liu, D. Zhang, Y. He, X. Zhao and R. Bai, *J. Membr. Sci.*, 2010, **346**, 121–130.
51 D. F. Rodrigues and M. Elimelech, *Environ. Sci. Technol.*, 2010, **44**, 4583–4589.
52 *Nanocyl, Biocyl*, http://www.nanocyl.com/kr/Products-Solutions/Products/BIOCYL.
53 A. Beigbeder, P. Degee, S. L. Conlan, R. J. Mutton, A. S. Clare, M. E. Pettitt, M. E. Callow, J. A. Callow and P. Dubois, *Biofouling*, 2008, **24**, 291–302.
54 R. J. Narayan, C. Berry and R. Brigmon, *Mater. Sci. Eng., B*, 2005, **123**, 123–129.
55 V. Vatanpour, S. S. Madaeni, R. Moradian, S. Zinadini and B. Astinchap, *J. Membr. Sci.*, 2011, **375**, 284–294.
56 A. Tiraferri, C. D. Vecitis and M. Elimelech, *ACS Appl. Mater. Interfaces*, 2011, **3**, 2869–2877.
57 T. Nguyen, B. Pellegrin, L. Mermet, A. Shapiro, X. Gu and J. Chin, *Nanotechnology*, 2009, 90–93.
58 T. Nguyen, B. Pelligrin, C. Bernard, X. Gu, J. M. Gorham, P. Stutzman, D. Stanley, D. Shapiro, E. Bryrd, R. Hettenhouse and J. Chin, *J. Phys.: Conf. Ser.*, 2011, **34**, 012060.
59 J. E. Guillet, T. W. Regulski and T. B. McAneney, *Environ. Sci. Technol.*, 1974, **8**, 923–925.
60 P. H. Jones, D. Prasad, M. Heskins, M. H. Morgan and J. E. Guillet, *Environ. Sci. Technol.*, 1974, **8**, 919–923.
61 W.-C. Chiang, C. Schroll, L. R. Hilbert, P. Moeller and T. Tolker-Nielsen, *Appl. Environ. Microbiol.*, 2009, **75**, 1674–1678.
62 D. Sun, S. Cheng, A. Wang, F. Li, B. E. Logan and K. Cen, *Environ. Sci. Technol.*, 2015, **49**, 5227–5235.
63 R. A. Gross and B. Kalra, *Science*, 2002, **297**, 803–807.
64 V. Massardier-Nageotte, C. Pestre, T. Cruard-Pradet and R. Bayard, *Polym. Degrad. Stab.*, 2006, **91**, 620–627.
65 C. Lefevre, A. Tidjani, W. C. Vander and C. David, *J. Appl. Polym. Sci.*, 2002, **83**, 1334–1340.
66 V. K. Khatiwala, N. Shekhar, S. Aggarwal and U. K. Mandal, *J. Polym. Environ.*, 2008, **16**, 61–67.
67 E. Werner, F. Roe, A. Bugnicourt, M. J. Franklin, A. Heydorn, S. Molin, B. Pitts and P. S. Stewart, *Appl. Environ. Microbiol.*, 2004, **70**, 6188–6196.
68 K. D. Xu, P. S. Stewart, F. Xia, C.-T. Huang and G. A. McFeters, *Appl. Environ. Microbiol.*, 1998, **64**, 4035–4039.
69 M. T. Madigan, J. M. Martinko, P. V. Dunlap and D. P. Clark, *Brock Biology of Microorganisms*, Pearson, San Francisco, 12th edn, 2009.
70 B. L. Allen, G. P. Kotchey, Y. N. Chen, N. V. K. Yanamala, J. Klein-Seetharaman, V. E. Kahan and A. Star, *J. Am. Chem. Soc.*, 2009, **131**, 17194–17205.
71 J. Russier, C. Ménard-Moyon, E. Venturelli, E. Gravel, G. Marcolongo, M. Meneghetti, E. Doris and A. Bianco, *Nanoscale*, 2011, **3**, 893–896.
72 L. Hall-Stoodley, J. W. Costerton and P. Stoodley, *Nat. Rev. Microbiol.*, 2004, **2**, 95–108.
73 A. R. Horswill, P. Stoodley, P. S. Stewart and M. R. Parsek, *Anal. Bioanal. Chem.*, 2007, **387**, 371–380.
74 Invitrogen, Molecular Probes, 2009, *FilmTracer LIVE/DEAD Biofilm Viability Kit*, Catalog No. L10316.
75 M. Vorregaard, *Technical University of Denmark, DTU, DK-2800 Kgs*, Lyngby, Denmark, 2008.
76 A. Heydorn, A. T. Nielsen, M. Hentzer, C. Sternberg, M. Givskov, B. K. Ersbøll and S. Molin, *Microbiology*, 2000, **146**, 2395–2407.
77 A. R. Boccaccini, J. Cho, J. A. Roether, B. J. Thomas, E. J. Minay and M. S. Shaffer, *Carbon*, 2006, **44**, 3149–3160.
78 H. Liu, L. Zhang, P. Shi, Q. Zou, Y. Zuo and Y. Li, *J. Biomed. Mater. Res., Part B*, 2010, **95**, 36–46.
79 M. E. McGovern, K. M. R. Kallury and M. Thompson, *Langmuir*, 1994, **10**, 3607–3614.
80 P. H. Mutin, G. Guerrero and A. Vioux, *J. Mater. Chem.*, 2005, **15**, 3761–3768.
81 J. E. Song, T. Phenrat, S. Marinakos, Y. Xiao, J. Liu, M. R. Wiesner, R. D. Tilton and G. V. Lowry, *Environ. Sci. Technol.*, 2011, **45**, 5988–5995.
82 M. Sodagari, H. Wang, B.-M. Z. Newby and L.-K. Ju, *Colloids Surf., B*, 2013, **103**, 121–128.
83 H. Wang, M. Sodagari, Y. Chen, X. He, B.-M. Z. Newby and L.-K. Ju, *Colloids Surf., B*, 2011, **87**, 415–422.
84 S. E. Page, J. R. Logan, R. M. Cory and K. McNeill, *Environ. Sci.: Processes Impacts*, 2014, **16**, 807–822.
85 W. R. Haag and J. Hoigné, *Chemosphere*, 1985, **14**, 1659–1671.
86 W.-C. Hou, S. BeigzadehMilani, C. T. Jafvert and R. G. Zepp, *Environ. Sci. Technol.*, 2014, **48**, 3875–3882.
87 R. M. Atlas, *Handbook of media for environmental microbiology*, CRC press, 2005.
88 D. M. Goeres, M. A. Hamilton, N. A. Beck, K. Buckingham-Meyer, J. D. Hilyard, L. R. Loetterle, L. A. Lorenz, D. K. Walker and P. S. Stewart, *Nat. Protoc.*, 2009, **4**, 783–788.
89 K. Schwartz, R. Stephenson, M. Hernandez, N. Jambang and B. R. Boles, *J. Visualized Exp.*, 2010, e2470.
90 T. R. Neu and J. R. Lawrence, *FEMS Microbiol. Ecol.*, 1997, **24**, 11–25.
91 J. Lawrence, D. Korber, T. Neu, C. Hurst, R. Crawford, J. Garland, D. Lipson, A. Mills and L. Stetzenbach, *Man. Environ. Microbiol.*, 2007, 40–68.
92 *Comstat 2 Homepage*, www.comstat.dk.
93 E. J. Petersen, T. Lam, J. M. Gorham, K. C. Scott, C. J. Long, D. Stanley, R. Sharma, J. Alexander Liddle, B. Pellegrin and T. Nguyen, *Carbon*, 2014, **69**, 194–205.
94 L. Chu and J. Wang, *Chemosphere*, 2013, **91**, 1310–1316.

95 M. Kubota, M. Matsui, H. Chiku, N. Kasashima, M. Shimojoh and K. Sakaguchi, *Appl. Environ. Microbiol.*, 2005, **71**, 8895–8902.
96 V. R. Hill, A. L. Polaczyk, D. Hahn, J. Narayanan, T. L. Cromeans, J. M. Roberts and J. E. Amburgey, *Appl. Environ. Microbiol.*, 2005, **71**, 6878–6884.
97 Y. Zheng, E. K. Yanful and A. S. Bassi, *Crit. Rev. Biotechnol.*, 2005, **25**, 243–250.
98 M. Kolybaba, L. Tabil, S. Panigrahi, W. Crerar, T. Powell and B. Wang, *The Proceedings of American Society of Agricultural Engineers (ASAE) Meeting*, North Dakota, USA, Paper No. RRV03-0007, October 3–4, 2004, pp. 1–15.
99 A. A. Shah, F. Hasan, A. Hameed and S. Ahmed, *Biotechnol. Adv.*, 2008, **26**, 246–265.
100 P. R and M. Doble, *Indian J. Biotechnol.*, 2005, **4**, 186–193.
101 K. Leja and G. Lewandowicz, *Pol. J. Environ. Stud.*, 2010, **13**, 255–266.
102 T. Ishigaki, W. Sugano, A. Nakanishi, M. Tateda, M. Ike and M. Fujita, *Chemosphere*, 2004, **54**, 225–233.
103 M. Shimao, *Curr. Opin. Biotechnol.*, 2001, **12**, 242–247.

